

Properties of heat-treated calcium phosphate coatings deposited by high-velocity oxy-fuel (HVOF) spray

H. Li^{a,*}, K.A. Khor^a, P. Cheang^b

^a*School of Mechanical & Production Engineering, School of Materials Engineering, Nanyang Technological University, Nanyang Avenue, Singapore 639798, Singapore*

^b*School of Materials Engineering, Nanyang Technological University, Nanyang Avenue, Singapore 639798, Singapore*

Received 15 November 2000; accepted 1 September 2001

Abstract

The influence of crystallization, upon heat treatment, on the properties of high-velocity oxy-fuel (HVOF) sprayed hydroxyapatite (HA) coatings was investigated. The characterization of the HA coating was performed by X-ray diffraction (XRD) and Fourier Transform Infrared Spectroscopy (FTIR). Differential Scanning Calorimeter (DSC) was employed to determine the crystallization temperature of the amorphous phase in an as-sprayed HA coating. The study demonstrated the effect of crystallization on the coating properties by considering the changes in materials chemistry, crystallinity level, and mechanical performance. Results showed that complete crystallization of the amorphous phase occurred at approximately 700°C and the crystallization temperature was dependent on sample heating rate in the DSC test. The changes of ion groups were detected by FTIR, before and after the phase transformation. The crystallization of the coating after annealing at 750°C resulted in a significant increase of the coatings' adhesive strength and shear strength, which attained maximum values 34 ± 3 and 14.1 ± 0.8 MPa, respectively. Young's modulus increased from 21 ± 1 to 25 ± 2 GPa. Microhardness measurements confirmed the changes in coating properties. It is also found that the transformation from the amorphous phase has crystalline HA as the only resultant phase detected by XRD. © 2002 Elsevier Science Ltd. All rights reserved.

Keywords: HVOF; Hydroxyapatite coating; Crystallization; Young's modulus; Adhesive strength; Shear strength

1. Introduction

Hydroxyapatite (HA) coatings deposited on titanium alloy substrates have the ability to induce new bone in-growth and subsequently increase fixation stability and, thus, are widely used in clinical applications. Among the problems experienced by HA coatings in contact with tissue, loosening is common [1]. It is believed that the amorphous phase, which has higher solubility than crystalline HA [2], in the coatings, can accelerate the fixation of the implant with the bony tissues and promote fast bone remodelling and attachment [3]. But a high content of amorphous phase in the coating can cause excessive dissolution and consequently reduce the reliability of the implants. Furthermore, the existence of immoderate amorphous phases at the interface of the HA deposit and metal alloy implant could be detrimental to the long-term survivability of

the implant as the interface may come into direct contact with bony tissues some period after implantation [4]. Therefore, post-spray treatment is needed to crystallize the amorphous phase and remove transitional or high-temperature phases from the coatings [5]. Among the processes adopted, heat treatment was thought of as one of the most effective methods, and has received much attention [6–9]. Controlling the amount and the location of the amorphous phase is very important for the proper functioning of the coated appliance.

Previous studies have shown that the presence of water vapor, hydrostatic pressure, or a combination of these could promote the crystallization of hydroxyapatite, which is composition dependent [10,11]. Furthermore, heat treatment in vacuum at a relatively high temperature, such as 950°C, can induce chemical reaction at the HA/Ti–6Al–4V interface with titanium phosphide as the resultant compound, detected by transmission electron microscope (TEM) analysis [12].

*Corresponding author.

This phenomenon can be the proof of the diffusion of Ti or P elements at the coating/substrate interface. While Filiaggi et al. [13] believed that increases in mechanical properties after heat treatment on the as-sprayed coatings were attributed to diffusion at the interface. However, the reported results focused mostly on changes of phase composition and microstructure [6,8,14–16], as well as the mechanism of the crystallization [10]. The influence of post-spray heat treatment on the mechanical properties of the hydroxyapatite coatings has not been studied. Furthermore, the crystallization temperature of the as-sprayed HA coatings differs to a certain extent depending on the characteristics of the raw HA powder and the spray system employed. Even though the transformation point from an amorphous phase to crystalline HA is generally determined, there are still reports that suggest that the crystallization can occur at low temperatures if extremely long isothermal treatment condition is satisfied [9].

High-velocity oxy-fuel (HVOF) technique has been widely used mainly due to its high flame velocity (up to Mach 5) and moderate temperature (below 3000°C). The moderate flame temperature is especially suitable for coating deposition of materials with low melting temperatures or low phase transformation points. In recent years, the HVOF process [17,18] has produced HA coatings with low content of amorphous calcium phosphate (ACP). However, the influence of recrystallization of the amorphous phase on coating properties of HVOF-sprayed calcium phosphate coatings is not known. In the present paper, calcium phosphate coatings with limited amorphous phase content were prepared by HVOF. The mechanical properties, which include Young's modulus, adhesive strength and shear strength, before and after heat treatment were investigated. Fourier Transform Infrared Spectroscopy (FTIR) and X-ray diffraction (XRD) techniques characterized the coatings.

2. Materials and experimental procedures

2.1. Materials, HVOF system and spray parameters

Spray-dried HA powders were made by a wet chemical method with a mean size of 30 µm and the particle size that ranged from 20 to 45 µm was used for the coating deposition on Ti–6Al–4V substrates. XRD analysis, which is shown in Fig. 1, reveals that the starting powders were composed of fully crystalline HA ($\text{Ca}_{10}(\text{PO}_4)_6(\text{OH})_2$) with a Ca/P ratio of 1.67 that is determined by EDX. The HV2000 HVOF (Praxair, USA) system with a nozzle diameter of 19 mm was used for the coating preparation. Hydrogen was utilized as the fuel gas with a flow rate of 566 dm³/min. The flow rate of oxygen was 283 dm³/min. Powder carrier gas was

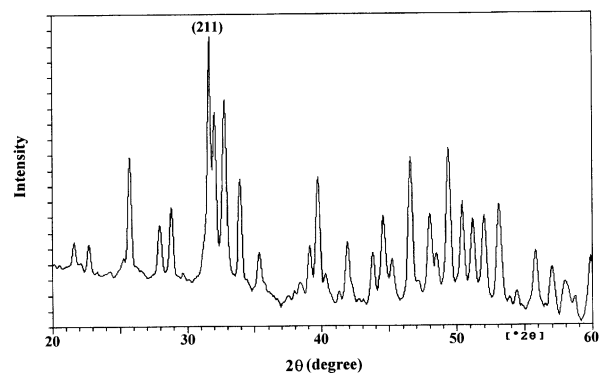


Fig. 1. XRD pattern of the starting HA powders showing the sole component of HA.

argon with a flow rate of 19 dm³/min. The spray distance was set at 250 mm.

2.2. Experimental methods

2.2.1. Annealing heat-treatment of HA coatings

The as-sprayed HA coatings were heat-treated in an annealing furnace. The samples were heated to 500° and 750°C, respectively, with a heating rate of 15°C/min, held for 30 min, and then slowly cooled back to room temperature within the furnace. The heating and cooling were performed in air atmosphere.

2.2.2. Phase analysis and relative crystallinity of HA

The phase composition of the starting powder and the as-sprayed coating, as well as the heat-treated coating, was analyzed by means of XRD (MPD 1880, Philips, the Netherlands). The operating conditions were 40 kV and 30 mA by using Cu K_α. The goniometer was set at a scan rate of 0.015° 2θ/s over a 2θ range of 20–60°. The true crystallinity value of thermal-sprayed coatings or powders was defined as the ratio of the crystalline regions to the sum of both crystalline and amorphous regions. However, this definition of crystallinity is hardly achievable, as there is no standard HA sample where the amorphous regions are clearly depicted and known. Therefore, the concept of relative crystallinity was accepted and used. In this case, spray-dried HA sample was chosen as a standard based on crystallinity and phase purity. The relative crystallinity (C_r) was calculated by comparing the highest peak, that is the (211) peak, of the powders or coatings with the (211) peak of the assumed standard reference HA sample. The mathematical expression is as follows:

$$C_r = \frac{A_{(211)}}{A_{s(211)}} \times 100\%, \quad (1)$$

where C_r is the relative crystallinity of the measured HA sample, $A_{(211)}$ the integrated area intensity of the (211) peak of HA powders or coatings and $A_{s(211)}$ the

integrated area intensity of the (211) peak of the assumed HA standard.

The relativity of the crystallinity only acts as a superficial gauging tool towards the determination of the crystallinity of a coating. It does not give a true indication of the crystallinity value, as decomposition of HA during thermal spraying is inevitable. In the present study, the XRD pattern of the starting HA powders was used as the reference based on that the powders showed nearly totally crystallized structure.

2.2.3. Differential Scanning Calorimeter (DSC) analysis

DSC analysis (Netzsch Thermal Analysis, DSC 404C) was performed to investigate the crystallization temperature of the as-sprayed HVOF HA coating. In order to reveal the effect of heating rate on the thermal behavior of HA, the samples were heated at a rate of 5°C/min and 10°C/min, respectively, to 1500°C in nitrogen atmosphere with a flow rate of 150 cm³/min.

2.2.4. Fourier Transform Infrared (FTIR) spectroscopy analysis

FTIR analysis (Nicolet Magna FTIR-560) was performed to characterize the change of the ion groups in the materials. The infrared spectrum with a resolution of 8 cm⁻¹ and the scan number of 4 was adopted with the scan range 400–4000 cm⁻¹.

2.2.5. Adhesive strength

The adhesive strength of the HA coating on the Ti–6Al–4V substrates was measured according to the ASTM C633-79 standard. Five samples were utilized for the determination of adhesive strength according to the standard. The HA coating thickness was 180 ± 15 μm and the tensile cross-head speed was set as 1 mm/min.

2.2.6. Shear strength

Specimens for the measurement of shear strength of HA coating to the metallic substrate were fabricated in-house, as schematically depicted in Fig. 2. In order to ensure the symmetry of the samples during the tensile procedure, the specimen was double sprayed with the same coating thickness on both sides, which can be easily achieved by the robot-controlled spray system. The thickness of the substrate was 2 mm and the coating area was 30 mm × 20 mm in width and length, respec-

tively. The coating thickness on each side of the substrate was 80 μm. If the specimen with HA coatings on both sides was bonded by two coupled specimens then the tensile test was performed on the Instron universal testing machine. The tensile speed was adopted as 0.2 mm/min. According to the maximum load, P , at which point fracture occurs, the shear strength can be calculated as follows:

$$\tau = \frac{P}{2ab}. \quad (2)$$

Six samples were used for the determination of shear strength for each type of coating.

2.2.7. Young's modulus

Young's modulus of HA coating was determined through a three-point bending test, which was firstly applied by Fawcett to thick films [19]. For the double-face sprayed specimen, which was expected to confirm to the symmetry during the bending to ensure maintenance of the neutral axis, the following formula was used to calculate Young's modulus E :

$$2E_c I_c + E_s I_s = \frac{Pl^3}{48d} \quad (3)$$

where I is inertia moment, P and d are the load and corresponding displacement of the load point in the elastic scope during the bending test. l is the span. The subscript c and s represent the coating and the substrate, respectively, and

$$I_s = \int_{-h_s/2}^{h_s/2} y^2 b \, dy, \quad I_c = \int_{h_s/2}^{(h_s/2)+h_c} y^2 b \, dy. \quad (4)$$

In the present study, the substrate thickness $h = 2$ mm, sample length was 120 mm. The bending span $l = 60$ mm and a bending speed of 0.2 mm/min was used. Young's modulus of Ti–6Al–4V used in this study was 113 GPa. The coating thickness, h_c , was around 150 μm. For the purpose of accurately determining Young's modulus of HA coatings, the coating thickness was accurately measured after the bending test by cutting the sample through a diamond blade. Accurate measurement was performed under microscope. For each set of data, three samples were used. Each sample was tested three times at different positions.

3. Results and discussion

3.1. Phase characterization

The XRD pattern of as-sprayed HA coating is shown in Fig. 4(a). It is found that a certain amount of amorphous phase exists in the as-sprayed coating besides the presence of α -tricalcium phosphate (α -TCP) and limited β -TCP. The relative crystallinity of the

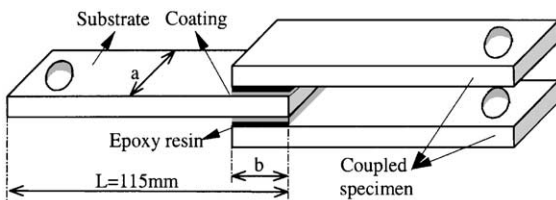


Fig. 2. Schematic depiction of the shear strength testing.

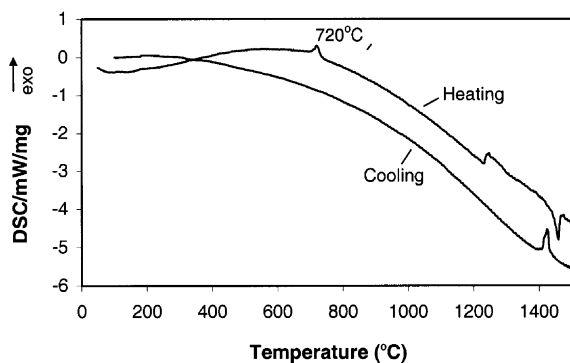


Fig. 3. DSC heating and cooling curves of the HA coating with a rate of $10^{\circ}\text{C}/\text{min}$ showing the crystallization temperature of ACP is around 720°C under the present DSC conditions.

coating was evaluated to be 41%. In order to determine the recrystallization temperature of the amorphous phase, DSC analysis was performed. The DSC curves shown in Fig. 3 reveal that, as the heating rate is $10^{\circ}\text{C}/\text{min}$, the crystallization temperature of the amorphous phase in HA coating is around 720°C , which is determined from the exothermal peak relating the exothermal characteristic of the crystallization. As the heating rate of the coating sample in the DSC test was $5^{\circ}\text{C}/\text{min}$, the peak assigned to the crystallization appeared at around 703°C , which claims the remarkable influence of heating rate on the tested point. The crystallization temperature of the ACP in HVOF sprayed HA coating is consistent with HA coatings deposited by plasma spraying [10]. The endothermal peak labeled at around 1457°C , shown in Fig. 3, would be the point where further transformation of residual HA [27] or oxyapatite [20] occurs. The ‘bump’ in the DSC heating curve at around 1031°C could suggest that the dehydration of HA starts to take place [21]. It is noted that for the HA coating, the cooling curve shown in Fig. 3 demonstrates a peak at around 1440°C . It may refer to the reversed full phase transformation from unstable $\bar{\alpha}$ -TCP to α -TCP [20]. The α -TCP comes from the transformation of $\bar{\alpha}$ -TCP at elevated temperatures [20,22].

In order to confirm the crystallization temperature, which is suggested to be around 700°C by the DSC results, post-spray heat treatment for the as-sprayed coatings was performed. The coatings were heated and cooled in the furnace with a 30 min hold at two temperatures, 500°C and 750°C , respectively. The influence of heat treatment on phase composition of the HA coating is shown in Fig. 4 with comparison to the as-sprayed coating. The XRD patterns of annealed coatings correspond to the results of DSC test. The heat treatment at 500°C did not transform the amorphous phase in the as-sprayed coating to crystalline HA, but the treatment at 750°C achieved this objective. It should

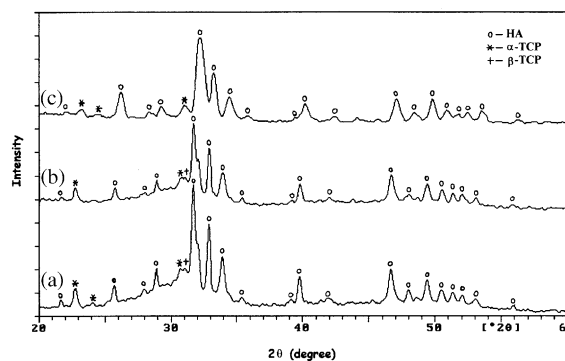


Fig. 4. XRD patterns of heat-treated HA coatings under (b) 500°C and (c) 750°C annealing with the comparison to (a) the as-sprayed coating.

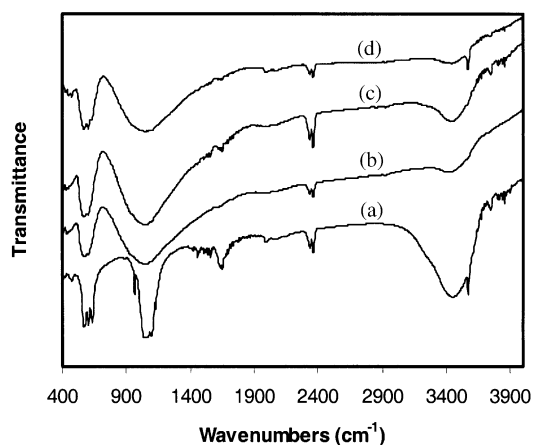


Fig. 5. IR spectra of HA powders and coatings annealed under different temperatures. (a) HA powders, (b) as-sprayed HA coating, (c) 500°C treated coating, and (d) 750°C treated coating.

be noted that the content of α -TCP remained unchanged and no other phase is detected in the fully crystallized coating, which suggests that the transformation from amorphous to crystalline phase only results in crystalline HA. The disappearance of β -TCP could be attributed to its transformation to α -TCP. This treatment is preferable in terms of phase composition of HA coatings to crystallize the amorphous phase while effectively inhibiting further decomposition of HA into tetracalcium phosphate (TTCP), which was revealed in HA coatings heat-treated at 950°C [23].

Fig. 5 demonstrates the FTIR results that indicate the change in the chemistry of the HA coatings before and after heat treatment. Significant differences can be found through the absence or presence of some peaks used for the determination of certain chemical groups. The bands at 3570 and 630 cm^{-1} were derived from the stretching and hindered rotation modes of hydroxyl (OH^-) group in HA powder. These are very sharp, indicating that the powder is indeed well crystallized. The sharp peak at 1649 cm^{-1} and those around 3447 cm^{-1} are indicative of

adsorbed water. The carbonate peaks that are located at 2000–2500 cm^{-1} result from the background carbon dioxide (CO_2) within the atmosphere. The disappearance of the OH^- -stretching mode at around 3570 cm^{-1} shown in Fig. 5(b,c) suggests the decreased content of crystallized HA according to Wang et al. [24]. The broad peak around 1000 cm^{-1} discloses the existence of the amorphous phase, which can be determined, when combined with the absence of the OH^- band. The changes of PO_4^{3-} are also exposed. The peaks labeled at 569 and 600 cm^{-1} indicate the bending mode PO_4^{3-} and those labeled at 958 and around 1090 cm^{-1} represent the stretching vibration mode PO_4^{3-} .

The as-sprayed HA coating almost does not reveal the OH^- peaks, neither does the coating treated at 500°C. The crystallized material following annealing treatment exhibits the presence of the OH^- group and the sharpening of the peaks relates to the existence of mostly crystalline HA materials (Fig. 5d). The XRD result shows that the amount of α -TCP in all the coatings is constant, thus this observation can be used to explain the FTIR spectra. That is, the crystallization treatment can make the OH^- group and PO_4^{3-} become prominent in the FTIR spectrum. This corresponds well with the results of XRD analyses.

From the XRD results in Fig. 4, it can be implied that the amorphous phase transformed only to crystalline HA. Through the investigation of the crystallization of amorphous calcium phosphate by Vogel et al. [9], it was postulated that the thermal decomposition of HA during plasma spraying is reversible when annealed at more than 600°C for 3 h in the presence of water vapor. But the present study only reveals the reversible trend between crystalline HA and amorphous calcium phosphate. No obvious phenomenon shows the participation of TCP in the reversible reaction.

It has been reported that the amorphous phase consists particularly of a dehydroxylated calcium phosphate [10]. The present study suggests the same possible composition of the amorphous calcium phosphate. It has been clearly understood that the crystallization of hydroxyl-rich areas produces hydroxyapatite, followed by diffusion of the hydroxyl ions [10], thus increasing the amount of the crystalline phase. Because the heat-treatment is performed in air, the humidity is enough to trigger the transformation from amorphous phase to crystalline HA upon cooling from 750°C.

3.2. Mechanical properties

The influence of the heat treatment on the mechanical performances in terms of adhesive strength and shear strength is shown in Fig. 6. The adhesive strength is significantly improved by the heat treatment at 750°C, increasing from 26 ± 2 MPa for the as-sprayed coating to

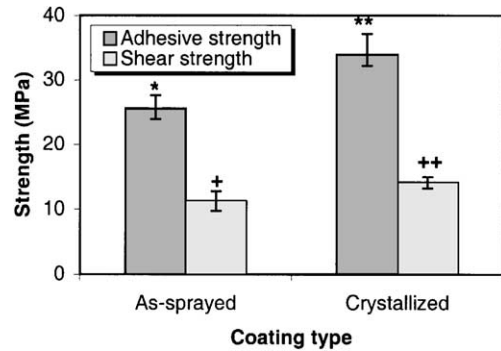


Fig. 6. Influence of crystallization on the adhesive strength and shear strength of HA coatings. ** vs *: $p < 0.05$, ++ vs +: $p > 0.05$.

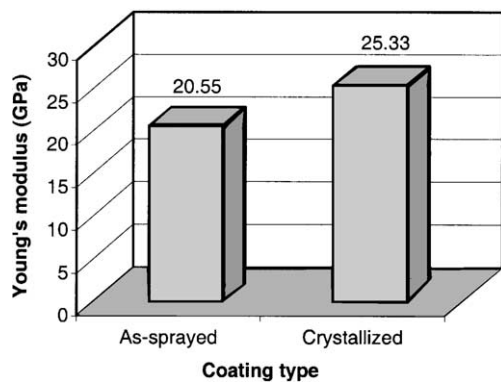


Fig. 7. Influence of crystallization treatment on Young's modulus of HA coatings, the standard deviation of as-sprayed coating is 1.36 GPa, and 2.04 GPa for crystallized coating. (Significantly different with $p < 0.05$.)

34 ± 3 MPa. The shear strength is also increased from 11.2 ± 0.9 to 14.1 ± 0.8 MPa.

Through the three-point bending test, the change in Young's modulus caused by crystallization is shown in Fig. 7. Remarkable increase was revealed. Generally, the fracture toughness of thermally sprayed coating is significantly dependent on both its Young's modulus and its capability to impede crack propagation [25]. As for the thermally sprayed coating, the splats bonding ratio, which was believed to mostly contribute to interface density that determines the ability to inhibit crack propagation [26], is generally less than 30%. For the present HA coatings (both as-sprayed and heat treated), heat treatment could not obviously change the bonding ratio between splats which was mainly realized during splat formation. It could be claimed that the crystallization of the amorphous phase is beneficial towards the improvement of fracture toughness of the HA coatings.

In order to reveal the possible reasons for the property improvement introduced by additional crystallization of the amorphous calcium phosphate phase,

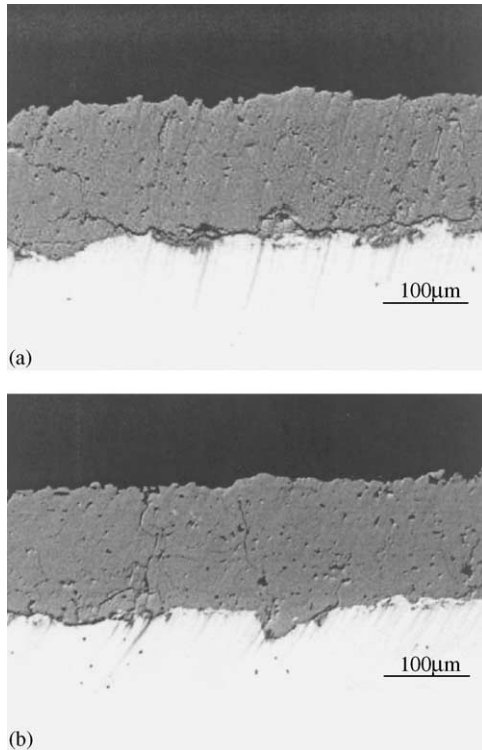


Fig. 8. Typical cross-sectional morphology of HA coatings. (a) as-sprayed coating; (b) crystallized coating. The microcracks existing within the coatings were caused by the polishing procedure as a result of the brittleness of the hydroxyapatite material.

microstructure and microhardness of HA coatings are investigated. Typical polished cross-sections of as-sprayed HA coating and correspondingly heat-treated coatings are shown in Fig. 8. It seems that no change in porosity can be deduced from the SEM images between as-sprayed and crystallized coatings. Improved interface owing to annealing heat-treatment can be observed.

The microhardness of as-sprayed HA coating and crystallized coating is shown in Fig. 9, in which the microhardness near the coating/substrate interface of a fully crystallized coating is also illustrated. The decrease of the microhardness of the crystallized coating, 1.0 ± 0.1 GPa, compared to that of original as-sprayed coating, 1.3 ± 0.1 GPa, suggests a change in brittleness owing to the heat treatment. Generally, the annealing treatment at 750°C is capable of releasing the residual stresses generated during coating deposition. It is also possible that the heat treatment at 750°C causes the diffusion between different splats. Thus, Young's modulus can be improved. Furthermore, the phase transformation is another important factor, which contributes to the improved Young's modulus because the different Young's moduli of the phases existing in the coating is one critical factor in determining Young's modulus of coating.

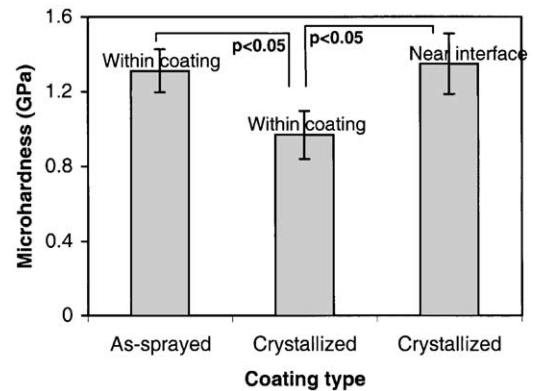


Fig. 9. Microhardness of as-sprayed and crystallized HA coatings.

It is found that Young's modulus of HVOF HA coatings obtained in the present study is lower than that of sintered bulk HA materials [27]. Metsger et al. [28] revealed that the Young's modulus of 1100°C sintered HA with full density was extremely low, thus they systematically demonstrated the inconsistent Young's modulus values of sintered HA materials produced at different temperatures, which were reported to vary from 10 to more than 100 GPa. The apparent rationale is that Young's modulus of HA materials is dramatically determined by the stress distributed in the material. This point can also be observed through the improvement of the fracture toughness which resulted from the release of residual stresses owing to the annealing treatment. While for HA coatings, owing to the inhomogeneous layered structure and pores which is thought of as a detrimental factor for Young's modulus [28], the low Young's modulus is in response to the microstructure with plenty of microcracks and unbonded zone among splats. Furthermore, even though the contraction was generally met after the crystallization by up to 1%, because of the different phase density of amorphous phase compared to crystal HA [10], it is still believed that the contraction cannot generate more cracks, and it is possible that residual tensile stresses are released.

The microhardness obtained in the heat-treated coating near the coating/substrate interface, 1.4 ± 0.2 GPa, is higher than that obtained away from the interface. This could be a concomitant effect, due to the diffusion or chemical reaction that occurs at the coating/substrate interface, and the improved interface shown in Fig. 8(b). Even though some phases, such as CaTi_2O_3 , CaO , could arise from the chemical reaction at the interface [12,29], the exact cause pointing to diffusion or chemical reaction cannot be decidedly determined by the EDX analysis alone. Considering the released residual stresses owing to annealing at an elevated temperature, some new phases near the interface zone could have contributed to the higher microhardness values. As the tensile fracture occurs at the coating side near the

coating/substrate interface, and the shear fracture locates mostly at the interface, the chemical reaction at the interface induced by the heat treatment seems to have a stronger claim as the dominant factor for the improved strength. Furthermore, some researchers have found that the content of amorphous phase near the HA coating/substrate interface was more than that in the coating due to the low thermal diffusivity of HA materials [30]. It is believed that the crystallization of the amorphous phase located near the coating/substrate has a positive effect on the adhesive strength and shear strength.

4. Conclusions

1. The crystallization temperature of the amorphous phase in HVOF-sprayed HA coating is determined by DSC to be around 700°C. XRD analysis confirms that the amorphous phase transformed directly to crystalline HA and not any other calcium phosphate phase. This led to the conclusion that minimal to negligible thermal decomposition of the HA phase took place during HVOF spraying.
2. The annealing heat-treatment at 750°C is beneficial for the improvement of adhesive strength and shear strength, as well as fracture toughness. Therefore, HVOF-sprayed HA coating do have to undergo post-spray treatment in the vicinity of 750°C.
3. The rapid solidification of crystalline HA as amorphous phase in HVOF-sprayed coating is reversible. No other phase is detected after the crystallization except the TCP that formed during coating deposition, whose overall phase content remained unchanged following heat treatment.
4. The relatively high microhardness values taken at the coating/substrate region is likely to be due to chemical reactions at the coating/substrate interface during the annealing treatment.

Acknowledgements

The authors would like to thank the technicians in Materials Lab of NTU for their help in experiments and Mr. Tan Boon Leng for his assistance in sample preparation, The financial support from Nanyang Technological University through research grant JT ARC 4/96 is also acknowledged.

References

- [1] Bonfield W. New trends in implant materials. In: Pizzoferrato A, Marchetti PG, Ravaglioli A, Lee AJC, editors. *Biomaterials and clinical applications*. Proceedings of the Sixth European Conference on biomaterials. Bologna, Italy, 1986. p. 13–21.
- [2] Ducheyne P, Radin S, King L. The effect of calcium phosphate ceramic composition and structure on in vitro behaviour: I. Dissolution. *J Biomed Mater Res* 1993;17:25–34.
- [3] Gross KA, Ben-Nissan B, Walsh WR, Swarts E. Analysis of retrieved hydroxyapatite coated orthopaedic implants. In: Coddet C, editor. *Thermal spray: meeting the challenges of the 21st century*. Proceedings of the 15th International Thermal Spray Conference. Nice, France, 1998. p. 1133–8.
- [4] Yang CY, Wang BC, Lee TM, Chang E, Chang GL. Intramedullary implant of plasma-sprayed hydroxyapatite coating: an interface study. *J Biomed Mater Res* 1997;36:39–48.
- [5] Khor KA, Cheang P. Effect of powder feedstock on thermal sprayed hydroxyapatite coatings. In: Berndt CC, Sampath S, editors. *Thermal spray: industrial applications*. Proceedings of the Seventh National Thermal Spray Conference. Boston, Massachusetts, USA, 1994. p. 147–52.
- [6] Kijk Kvan, Schaeken HG, Wolde JGC, Jansen JA. Influence of annealing temperature on RF magnetron sputtered calcium phosphate coatings. *Biomaterials* 1996;17:405–10.
- [7] Wang Y, Khor KA, Cheang P. Thermal spraying of functionally graded calcium phosphate coatings for biomedical implants. *J Therm Spray Technol* 1998;7:50–7.
- [8] Tong W, Yang Z, Zhang X, Yang A, Feng J, Cao Y, Chen J. Studies on diffusion maximum in X-ray diffraction patterns of plasma-sprayed hydroxyapatite coatings. *J Biomed Mater Res* 1998;40:407–13.
- [9] Vogel J, Russel C, Guntheer G. Characterization of plasma-sprayed hydroxyapatite by P-MAS-NMR and the effect of subsequent annealing. *J Mater Sci Mater Med* 1996;7:495–9.
- [10] Gross KA, Gross V, Berndt CC. Thermal analysis of amorphous phases in hydroxyapatite coatings. *J Am Ceram Soc* 1998;81:106–12.
- [11] Yamashita K, Arashi T, Kitagaki K, Yamada S, Ogawa K. Preparation of apatite thin films through rf sputtering from calcium phosphate glasses. *J Am Ceram Soc* 1994;77:2401–7.
- [12] Ji H, Marquis PM. Effect of heat treatment on the microstructure of plasma-sprayed hydroxyapatite coating. *Biomaterials* 1993;14:64–8.
- [13] Filiaggi MJ, Pilliar RM, Coombs NA. Post-plasma-spraying heat treatment of the HA coating/Ti-6Al-4V implant system. *J Biomed Mater Res* 1993;27:191–8.
- [14] Khor KA, Cheang P. Laser post-treatment of thermally sprayed hydroxyapatite coatings. In: Berndt CC, Sampath S, editors. *Thermal spray: industrial applications*. Proceedings of the Seventh National Thermal Spray Conference. Boston, Massachusetts, USA, 1994. p. 153–7.
- [15] Ranz X, Pawlowski L, Sabatier L, Sabatier L. Phases transformations in laser treated hydroxyapatite coatings. In: Coddet C, editor. *Thermal spray: meeting the challenges of the 21st century*. Proceedings of the 15th International Thermal Spray Conference. Nice, France, 1998. p. 1343–9.
- [16] Cao Y, Weng J, Chen J, Feng J, Yang Z, Zhang X. Water vapour-treated hydroxyapatite coatings after plasma spraying and their characteristics. *Biomaterials* 1996;17:419–24.
- [17] Wolke JGC, De Groot K, Kraak TG, Herlaar W, De Blicck-Hogervorst JMA. The characterization of hydroxyapatite coatings sprayed with VPS, APS and DJ system. In: Bernecki Tomas F, editor. *Thermal spray coatings: properties, processes and applications*. Proceedings of the fourth NTSC. Pittsburgh, USA 1991. p. 481–90.
- [18] Haman JD, Chittur KK. Four point bend testing of calcium phosphate coatings. Proceedings of 16th Southern Biomedical Engineering Conference 1997. p. 305–8.
- [19] Fawcett N. A novel method for the measurement of Young's modulus for thick-film resistor material by flexural testing of coated beams. *Mater Sci Technol* 1998;9:2023–6.

- [20] Zhou J, Zhang X, Chen J, Zeng S, de Groot K. High temperature characteristics of synthetic hydroxyapatite. *J Mater Sci Mater Med* 1993;4:83–5.
- [21] Liao C, Lin F, Chen K, Sun J. Thermal decomposition and reconstitution of hydroxyapatite in air atmosphere. *Biomaterials* 1999;20:1807–13.
- [22] Harris DH. Overview of problems surrounding the plasma spraying of hydroxyapatite coatings, In: Bernecki TF, editor. *Thermal spray research and applications*. Proceedings of the Third NTSC. Long Beach, CA, USA, May 1990. p. 419–23.
- [23] Brossa F, Cigada A, Chiesa R, Paracchini L, Consonni C. Post-deposition treatment effects on hydroxyapatite vacuum plasma spray coatings. *J Mater Sci Mater Med* 1994;5:855–7.
- [24] Wang BC, Chang E, Yang CY, Tu D, Tsai H. Characteristics and osteoconductivity of three different plasma-sprayed hydroxyapatite coatings. *Surf Coat Technol* 1993;58:107–17.
- [25] Beshish GK, Florey CW, Worzala FJ, Lenling WJ. Fracture toughness of thermal spray ceramic coatings determined by the indentation technique. *J Therm Spray Technol* 1993;2:35–8.
- [26] Callus PJ, Berndt CC. Relationships between the mode II fracture toughness and microstructure of thermal spray coatings. *Surf Coat Technol* 1999;114:114–28.
- [27] Aoki H. *Medical applications of hydroxyapatite*. Japan: Ishiyaku EuroAmerica, 1994.
- [28] Metsger DS, Rieger MR, Foreman DW. Mechanical properties of sintered hydroxyapatite and tricalcium phosphate ceramic. *J Mater Sci Mater Med* 1999;10:9–17.
- [29] Ueda M, Hayakawa H, Motoe A, Fujioto T, Mukaida M. Formation of Ti3P at the hydroxyapatite/titanium interface heated by radio-frequency thermal plasma of argon. In: Sudarsan TS, Khor KA, Jeandin M, editors. *Proceedings of the Tenth International Conference on Surface Modification Technologies*: Singapore, 1996. p. 728–36.
- [30] Gross KA, Berndt CC, Herman H. Amorphous phase formation in plasma-sprayed hydroxyapatite coatings. *J Biomed Mater Res* 1998;39:407–14.